Unsteady Reynolds averaged Navier-Stokes simulation of the post-critical flow around a closely spaced group of silos

J. Hillewaere[1], J. Degroote[2], J. Vierendeels[2], G. Lombaert[1], G. De Roeck[1], G. Degrande[1]
[1]Department of Civil Engineering, K.U.Leuven, Kasteelpark Arenberg 40, B-3001 Leuven, Belgium
[2]Department of Flow, Heat and Combustion Mechanics, Ghent University, St.-Pietersnieuwstraat 41, B-9000 Gent, Belgium
email: jeroen.hillewaere@bwk.kuleuven.be, joris.degroote@ugent.be, jan.vierendeels@ugent.be,
geert.lombaert@bwk.kuleuven.be, guido.deroeck@bwk.kuleuven.be, geert.degrande@bwk.kuleuven.be

ABSTRACT: During a storm in October 2002, wind induced ovalling oscillations were observed on several empty silos of a closely spaced group of 8 by 5 silos in the port of Antwerp (Belgium). Present day standards describe only basic wind load cases, unable to explain this ovalling phenomenon. In order to improve the design of engineering structures with cylinders placed in groups, a thorough understanding of the fluid flow around such groups is required. 2D unsteady Reynolds averaged Navier-Stokes (URANS) equations using Menter's shear stress transport turbulence model were performed, considering the wind flow around the rectangular group for a range of angles of incidence ($0^\circ \leq \alpha \leq 90^\circ$). The 2D highly turbulent post-critical flow ($\mathrm{Re} = 1.24 \times 10^7$) around a single cylinder was computed to elucidate the influence of the applied turbulence model and to validate the spatial and temporal discretization. Since, the flow regime around and within the silo group is similar to the flow around rectangular cylinders and the flow within tube arrays (e.g. heat exchangers), similarities and differences are used to assess the influence of the angle of incidence on the flow pattern around the cylinder group. The large velocities in the interstitial flow between cylinders as well as the formation of large scale vortex shedding in the wake of the group are discussed for various angles of incidence. Static and dynamic loadings on separate silos of the group are studied to explain the existence and the location of ovalling oscillations in closely spaced silo groups.

KEY WORDS: Circular cylinder; Cylinder group; Ovalling; Post-critical flow; Pressure coefficient.

1 INTRODUCTION AND MOTIVATION

Circular cylinders are encountered in civil engineering constructions as silos, (solar) chimneys, water towers, power transmission lines, offshore structures and suspension bridge cables. Although wind loading is an important design load for these structures, only basic wind load cases are described in standards, e.g. in Eurocode 1 [1]. Since the configuration and orientation of the group drastically change the fluid flow around the cylinders, a more realistic estimation of the pressure coefficients and forces is required. This can be provided by experimental or numerical simulations of the wind flow.

During a storm in October 2002, ovalling was observed on several empty silos on the corners of a group of forty silos in the port of Antwerp. The group is organized in five rows of eight very closely spaced silos (pitch to cylinder diameter ratio $= P/D = 1.05$). The silo group is situated in proximity of the river Scheldt in vast and flat surroundings and is therefore classified in terrain category II of Eurocode 1 [1]. The calculated mean wind velocity $v_\mathrm{f} = 31.8\,\mathrm{m/s}$ at half the height of the silo (30 m above ground level) consequently leads to a highly turbulent, post-critical flow regime at Reynolds number $\mathrm{Re} = v_\mathrm{f} D/\nu = 1.24 \times 10^7$ [2]. Because of the small spacing ratio between silos and the high Reynolds number, no experimental or numerical data applicable to this case are available.

Wind induced ovalling oscillations are an aeroelastic phenomenon where the cross section of the structure deforms as a shell without bending deformation with respect to the longitudinal axis of symmetry [3]. Prior to the study of wind-structure interaction, both structure and fluid behaviour should be studied. On the one hand, Dooms et al. [4] studied the ovalling mode shapes of the empty silo structures. Each ovalling mode shape is referred to by a couple (m,n) where m denotes the half wave number in the axial direction and n is the number of circumferential waves (figure 1). On the other hand, numerical simulations of the turbulent wind flow, modelled as incompressible (low Mach number) flow, are performed in the present paper to explain the occurrence of the observed ovalling oscillations in the 8 by 5 group. The influence of the angle of incidence α of the wind flow on these ovalling oscillations is examined. Other parameters such as spacing ratio, Reynolds number, etc. are left unchanged.

Details on the applied computational model are discussed in the next section. The less complex and better documented case of 2D flow around a single cylinder in the post-critical regime is considered to validate the numerical procedure. In the third section, the complex flow around the 8 by 5 silo group is analyzed. Similarities of the present flow with the flow within tube arrays (e.g. heat exchangers) and the flow around rectangular cylinders are discussed. Time averaged and fluctuating pressure coefficients as well as drag and lift forces are calculated to examine the influence of the angle of incidence ($0^\circ \leq \alpha \leq 90^\circ$). Finally, the existence of ovalling vibrations in cylinder groups is explained.

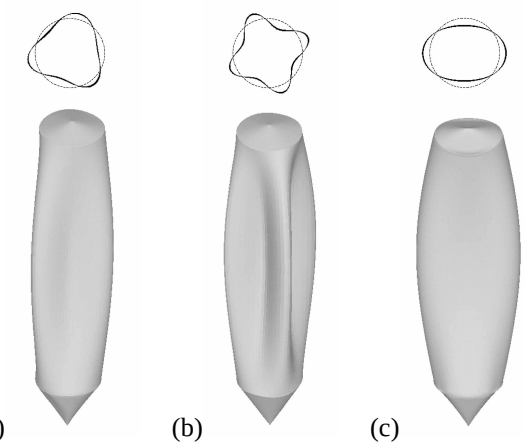

(a) (b) (c)

Figure 1. Selected ovalling eigenmodes of a single silo, (a) mode (1,3) at 3.93 Hz, (b) mode (1,4) at 3.93 Hz and (c) mode (1,2) at 7.75 Hz [4].

2 COMPUTATIONAL PROCEDURE AND VALIDATION

The simulation of highly turbulent flows around complex geometries is a computationally challenging task. Therefore, the case of a single cylinder in cross flow is calculated first in order to validate the computational model. This approach, known as the Building Block Approach and introduced by the AIAA [5], allows the validation of a proposed computational model with a simpler sub-system for which experimental data are available. The lack of experimental data for the 8 by 5 silo group makes this approach particularly interesting.

2.1 Numerical procedure

The choice of a particular numerical technique is mainly influenced by the complex geometry of the problem and the computational effort. The finite volume method (FVM) is used for the discretization of the governing incompressible Navier-Stokes equations, while for the numerical treatment of turbulence, the Reynolds averaged Navier-Stokes (RANS) procedure with the hybrid shear-stress transport (SST) turbulence model is chosen. The SST model, suggested by Menter, combines the robust and accurate formulation of the $k-\omega$ model in the near-wall region with the free stream independence of the $k-\varepsilon$ model in the far field and should therefore be more accurate and reliable for a wider class of flows [6]. The computational time required for RANS simulations is modest when compared to other techniques, e.g. large eddy simulations (LES) or detached eddy simulations (DES). For similar reasons, a 2D cross section of the silo group is considered. Although 3D flow simulations over complex bodies have become possible in recent years, they remain very expensive and are therefore limited to moderate Reynolds numbers. 2D simulations are quite feasible, even for complex geometries and relatively high Reynolds numbers [7].

To solve the 2D unsteady Reynolds averaged Navier-Stokes (URANS) discretized set of equations, a second order interpolation of the pressure, a second order upwind interpolation of momentum, turbulent kinetic energy k and specific dissipation rate ω are applied, while a second order implicit, unconditionally stable, time stepping method is used. To deal with the pressure-velocity coupling, a coupled pressure-based calculation is performed which, unlike segregated algorithms such as PISO or SIMPLE [5], is known for its significantly improved rate of convergence [6].

2.2 Computational domain and boundary conditions

The boundaries of the fluid domain should be sufficiently far from the near-wall region where accuracy is important: distances of $9D$ to the inlet and the lateral boundaries and $30D$ to the outlet of the domain are used, with D the diameter of the cylinder. Equivalently, $9D_\mathrm{g}$ and $30D_\mathrm{g}$ are used for the group configuration, with D_g the projected width of the silo group (figure 2).

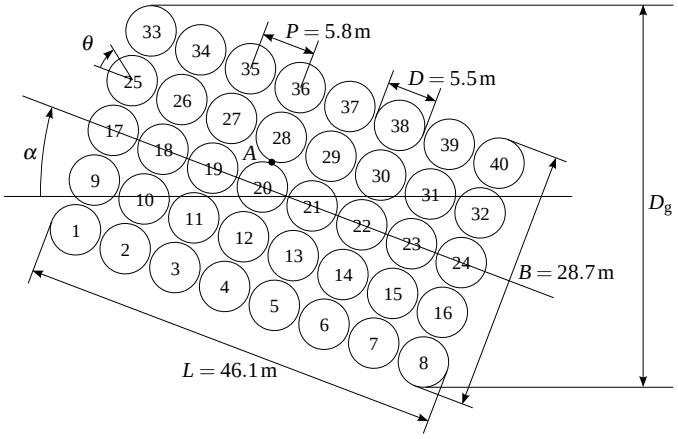

Figure 2. Plan view of the silo group with numbering of the invididual silos. Normative dimensions are given as well as definitions for the angle of incidence α and the angle θ on the circumference of an individual cylinder.

In the computations, the air density is $\rho = 1.25\,\mathrm{kg/m^3}$ and its dynamic viscosity is $\mu = 1.76\times10^{-5}\,\mathrm{Pa\,s}$. At the velocity inlet with imposed free stream velocity $v_\mathrm{f} = 31.8\,\mathrm{m/s}$, the turbulent energy k and specific dissipation rate ω have to be defined. Since values for k and ω cannot be determined from on site measurements, they are based on the turbulence intensity I and the turbulence length scale l [5]. A reasonably low turbulence intensity $I = 1\%$ is assumed and $k = 3(v_\mathrm{f}I)^2/2 = 0.152\,\mathrm{J/kg}$ at the inlet. Several researchers showed that turbulence at the upstream boundary results in very little difference in turbulence intensity in vicinity of the bluff body [8] [9]. The turbulence length scale l is typically chosen as a percentage of a characteristic dimension of the problem, e.g. $l = 0.06D_g = 1.8\,\mathrm{m}$ for $\alpha = 0^\circ$, and hence a dissipation rate $\omega = C_\mu^{-1/4}\sqrt{k}/l = 0.395\,\mathrm{s^{-1}}$ is imposed at the inlet with $C_\mu = 0.09$ a model constant. The entire flow field is initialized with these inlet conditions. The outlet boundary is modelled as a pressure outlet where the static pressure is set equal to the reference pressure. At the lateral boundaries symmetry is imposed. The cylinder walls are considered smooth and no-slip boundary conditions are applied.

2.3 Spatial and temporal grid refinement

For transient simulations, the governing equations must be discretized in both space and time. The verification of

convergence and grid independency is performed for the single cylinder case.

The near-wall treatment at the solid cylinder walls is the principal issue for spatial grid refinement: two distinct approaches can be applied. When a very fine mesh is used near the cylinder wall and the first grid point is located in the viscous sublayer, velocity gradients are computed explicitly. Alternatively, logarithmic wall functions can be used to model the near-wall behaviour, significantly reducing the number of elements and computation time. However, the first grid point should be sufficiently distant from the surface for viscous stresses to be negligible, yet sufficiently close so that inertial terms can be neglected. Several mesh configurations were processed to find an optimal refinement in the near-wall region, allowing to use the log-law functions.

Multiple time step refinements have also been performed and show that convergence is reached for a time step of approximately 0.00125 s. The computational efforts can be drastically reduced without changing the outcome fundamentally when a slightly larger time step $\Delta t = 0.005\,\mathrm{s}$ is applied in the simulations.

2.4 Validation of single cylinder simulations

Although the flow around a circular cylinder has been widely studied, very few experiments or computations have been performed for a flow in the post-critical regime. For validation, the present numerical results are compared with experimental data and results of other (2D and 3D) numerical simulations. Typical parameters for this comparison include the Strouhal number $\mathrm{St} = \mathrm{f_{vs}L/v_f}$, the separation angle θ_s (figure 3) and the pressure coefficient, with f_{vs} the vortex shedding frequency, v_f the free stream velocity of the fluid and L the characteristic length, equal to the diameter D of the cylinder in the present case. The pressure coefficient along the circumference of a cylinder at a certain point in time is defined as

$$C_p(\theta,t) = \frac{p(\theta,t) - p_f}{\rho v_f^2/2} \tag{1}$$

with p_f the free stream pressure. The time averaged pressure coefficient $\overline{C}_p$ is calculated as follows:

$$\overline{C}_p(\theta) = \frac{1}{N}\sum_{i=1}^{N} C_p(\theta,t) \tag{2}$$

with N the number of time steps. For the present simulation, the time averaged pressure coefficient is shown in figure 3 with $\theta_s = 116^\circ$ and $\mathrm{St} = 0.32$.

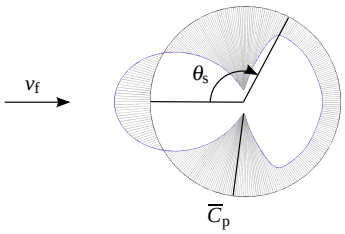

Figure 3. Time averaged pressure coefficient $\overline{C}_p(\theta)$ on the circumference of the cylinder with indication of the free stream velocity v_f and the separation angle θ_s.

Zdravkovich [2] gives an elaborate overview of experimental pressure coefficients at Reynolds numbers from 0.73×10^7 to 3.65×10^7 (figure 4). In the reported experiments, separation occurs between $\theta_s = 100^\circ$ and 110°. For Reynolds numbers larger than 0.5×10^7, experimental smooth flow data of Zan [10] indicate that the Strouhal number remains at 0.2, whereas Schewe [11] found that it rises to about 0.3 as the Reynolds number approaches 10^7; consistent with the tendency of the Strouhal number to rise from 0.2 to 0.3 in the range of Reynolds numbers between 10^6 and 10^7 [2].

Several numerical simulations have been reported in the literature for highly turbulent cross flows around circular cylinders. Younis et al. [12] performed 2D URANS simulations at $\mathrm{Re} = 0.35\times10^7$ with different turbulence models and report a Strouhal number of 0.28 and separation at $\theta_s = 120^\circ$. Travin et al. [13] applied 3D DES for Reynolds numbers up to 3×10^6 and found Strouhal numbers 0.35 with separation at $\theta_s = 111^\circ$.

All experimental and numerical data from literature show considerable scatter due to differences in Reynolds number, applied turbulence model, etc. However, it can be concluded that a generally good agreement is found between the present simulations ($\mathrm{St} = 0.32$, $\theta_s = 116^\circ$) and the data from literature. Figure 4 also shows that the pressure coefficient on the circumference of the cylinder is in generally good agreement with the experimental data gathered by Zdravkovich [2].

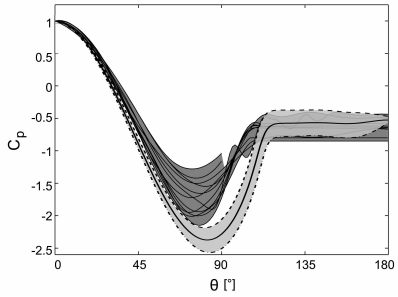

Figure 4. Measured pressure coefficients at Reynolds numbers from 0.73×10^7 to 3.65×10^7 [2] (dark grey zone) vs. present calculated maximal (dashed line), minimal (dash-dotted line) and time averaged pressure coefficients $\overline{C}_p(\theta)$ (solid line) at $\mathrm{Re} = 1.24\times10^7$.

3 TURBULENT AIR FLOW AROUND THE 8 BY 5 CYLINDER GROUP

The numerical procedure described in the previous section was applied for the turbulent air-flow around the 8 by 5 silo group for 7 angles of incidence ($0^\circ \le \alpha \le 90^\circ$), in order to clarify the observed ovalling vibrations on the corners of the group. A distinction is made between vibrations related to the periodicity of the interstitial flow between the cylinders and vibrations caused by the large vortex structures behind the entire cylinder bundle.

3.1 Discussion of the flow around the cylinder group

Figure 5c shows the instantaneous flow pattern for an angle of incidence $\alpha = 30^\circ$. At the transverse corner cylinders of the group (cylinders 33 and 8), shear layers in the outer flow

are separated while approximately 10% of the flow is forced through the interstitial spaces in the group. These interstitial flows emerge at the lee side, join up and form several local recirculation zones in the wake that coalesce as they are carried downstream. Eventually one large scale vortex street is formed in the wake of the entire group. The periodicity of this vortex street is depicted by the Strouhal number St, summarized in table 1 with characteristic length $L = D_g$. The decrease of the Strouhal number for the intermediate angles of incidence ($\alpha = 30^\circ$ to 60°, table 1 or figure 6) is due to the decrease in vortex shedding frequency for these angles. When the projected width of the cylinder group (D_g) is increased, the distance between the free shear layers increases, resulting in larger shedded vortices and lower shedding frequencies.

For the smallest angles of incidence ($\alpha = 0^\circ$ and 15°, figures 5a and 5b), it is clear that the emerging interstitial flows on the upper downstream side of the group (cylinders 33 to 40) are joined up and dragged downstream without forming local recirculation zones, due to the proximity of the separated shear layer. The same applies for the highest angles of incidence ($\alpha = 75^\circ$ and 90°), where no such recirculation zones can be formed on the lower side of the group (cylinders 8, 16, 24, 32 and 40).

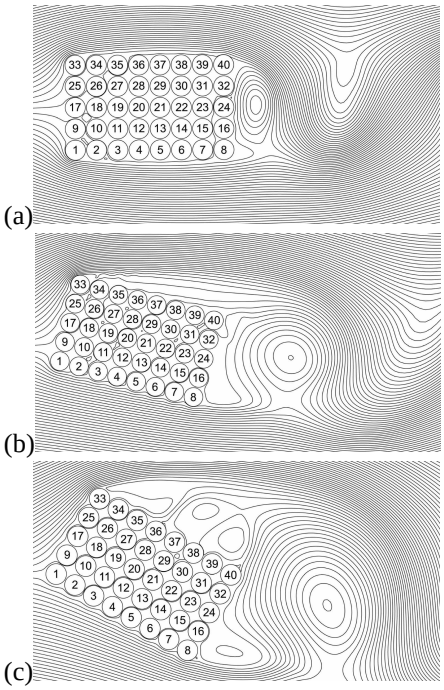

Figure 5. Velocity streamlines of the flow around the 8 by 5 cylinder group for an angle of incidence (a) $\alpha = 0^\circ$ at $t = 80.0$ s, (b) $\alpha = 15^\circ$ at $t = 82.5$ s and (c) $\alpha = 30^\circ$ at $t = 77.0$ s with flow coming from the left.

It is interesting that the flow around the group as a whole resembles the behaviour of a single bluff body in cross flow. Kareem et al. [14] found a similar behaviour for two closely spaced cylinders in tandem arrangement where separated shear layers interact and roll up to form one large scale vortex as well. In figure 6, the present results are therefore compared with experimental results of Knisely [15] for a rectangular cylinder ($L/B = 1.67$) in cross flow ($1.2 \times 10^4 \leq \mathrm{Re} \leq 2.4 \times 10^4$).

Table 1. Strouhal frequencies (f_{vs}) and Strouhal numbers (St) for all different angles of incidence (α) with respective projected width of the silo group (D_g).

α	[°]	0	15	30	45	60	75	90
D_g	[m]	28.7	38.4	45.9	50.6	52.3	50.7	46.1
T_{vs}	[s]	3.23	4.18	5.85	6.32	6.93	5.70	5.14
f_{vs}	[Hz]	0.31	0.24	0.17	0.16	0.14	0.18	0.20
St		0.28	0.29	0.25	0.25	0.23	0.29	0.29

Significant dependence of the shedding frequency on the angle of incidence is observed in the experimental results: the sudden rise and fall in Strouhal number for very small or high angles of incidence is interpreted as an indicator of the reattachment of the separated shear layer [15].

The present Strouhal numbers are significantly higher than the experimental results. Apart from a slightly different side ratio for the present simulations ($L/B = 1.6$), this discrepancy may be due to differences in four other parameters. Firstly, turbulence intensity levels are known to affect the angle of reattachment on a cylinder wall [16] but the effect on the Strouhal number is believed to be limited and related to the angle of incidence of the fluid flow. Only for low turbulence intensities, the Strouhal number might be slightly increased for small angles of incidence ($\alpha < 20^\circ$) [15] [17]. Secondly, the present simulations were performed at a much higher Reynolds number, possibly leading to an increase in the Strouhal number [15]. Thirdly, data on the effects of rounded corners of the rectangular cylinders are somewhat limited and scattered, but the general tendency for the Strouhal number is to increase with increasing rounding radius [15]. Finally, the most important difference between a bluff rectangular cylinder and the present cylinder group is the porosity of the latter. The emerging interstitial flows at the downstream side of the cylinder group prevent the shear layer from reattaching for very small and very high angles of incidence. This explains the absence of the sudden rise and fall in Strouhal number for the present simulations.

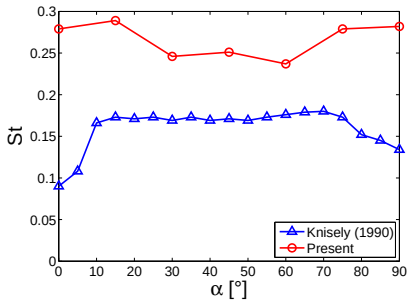

Figure 6. Comparison of Strouhal numbers for the present 8 by 5 silo group at $\mathrm{Re} = 1.24 \times 10^7$ and a rectangular cylinder with side ratio $L/B = 1.67$ at Re between 1.2 and 2.4×10^4 [16] for angles of incidence α between 0° and 90°.

3.2 *Discussion of the interstial flow in the cylinder group*

Despite important differences (e.g. close spacing between cylinders and limitation to 40 cylinders in the present simulation), the interstitial flow pattern in the present simulations can be

related to the flow through tube bundles that has been widely studied for the design of heat exchangers. These tube arrays are typically divided in two categories [18]: the in-line category where cylinders are arranged in square or rectangle arrays and the interstitial flow is mostly straight through the arrays and the staggered category where cylinders are arranged in rotated square or triangle arrays and the flow is forced along wavy paths. Depending on the angle of incidence, the present silo group could be classified in either category: the in-line, square configuration applies to the cases with $\alpha = 0^\circ$ and $\alpha = 90^\circ$ while for all other angles of incidence the staggered, rotated square arrangement would be applicable. As shown in figure 7, this is not always the case.

No straight flow pattern for $\alpha = 0^\circ$ (figure 7a) and $\alpha = 90^\circ$ is found. For in-line tube bundles, the presence of the subsequent row prevents the transitional eddies to form and roll-up and the eddies are carried away between the tubes by the jet-like interstitial flow [19]. The present cylinders, however, are too closely packed and the eddies partially or completely disappear in the distorted flow. Instead, the interstitial flow is not separated from the cylinder wall and follows a wavy path through the array, deflecting the flow up- and downward to the sides of the group, following the shortest path from the high pressures at the leading side of the group to the lower pressures at the lee side of the group. For other angles of incidence, interstitial flows resemble the wavy interstitial flow pattern of staggered tube bundles [18], e.g. for $\alpha = 30^\circ$ (figure 7b). However, for $\alpha = 60^\circ$ (figure 7c) and $\alpha = 15^\circ$ (not shown), the regular wavy pattern is interupted at arbitrary points in the array, where the interstitial flow separates from the cylinder surface and forms small recirculation zones or even results in local vortex shedding. As suggested by Mittal et al. [7], the presence of these irregularities may be directly related to the 2D character of the simulations, which would be canceled out in 3D simulations where spanwise velocities are allowed.

Other flow phenomena are similar for tube bundles and the present case. Several experiments on tube arrays [18] [20] show that turbulence intensity is built up as the interstitial flow proceeds through the array until the rate of turbulence generation is balanced by the turbulence dissipation. For the 8 by 5 cylinder group, turbulence is also generated in the cylinder array itself and attains maximal values at the upper and lower edges of the rectangular array, where turbulence generation and dissipation is high because of the high flow velocities.

Another similarity concerns the observation of several inter-related flow periodicities in staggered tube arrays in experiments [8] [21]. For the present cylinder group, multiple peaks in the frequency spectrum of the pressure were also observed through the array for all angles of incidence α, as shown in figure 8 for an arbitrary point A in the middle of the cylinder group (figure 2). These frequency peaks are located at multiples of the Strouhal frequency, which is identified at the dominant, lowest frequency peak. For $\alpha = 60^\circ$ (figure 8b), smaller peaks are detected at 6 Hz (similarly for $\alpha = 15^\circ$ at 2 Hz), which are related to the deviating wavy pattern for these angles of incidence (figure 7c). No specific pattern of the locations in the array where these irregular peaks occur, was found.

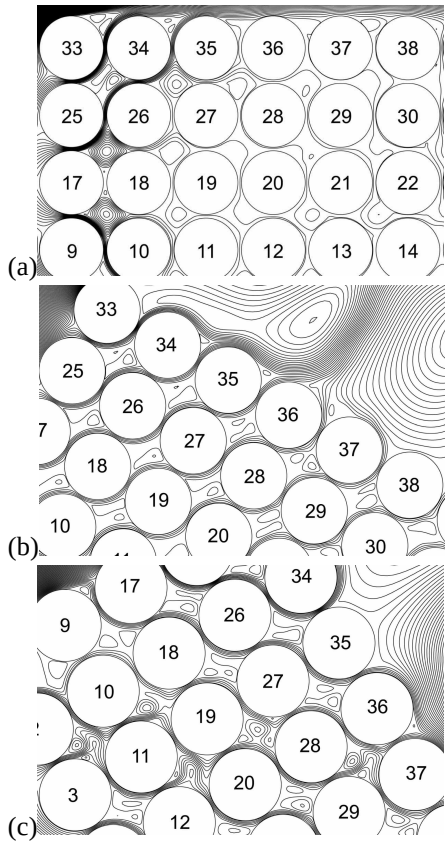

Figure 7. Detail of velocity streamlines for the interstitial space in the 8 by 5 cylinder group for an angle of incidence (a) $\alpha = 0^\circ$ at $t = 78.5$ s, (b) $\alpha = 30^\circ$ at $t = 79.0$ s and (c) $\alpha = 60^\circ$ at $t = 85.0$ s.

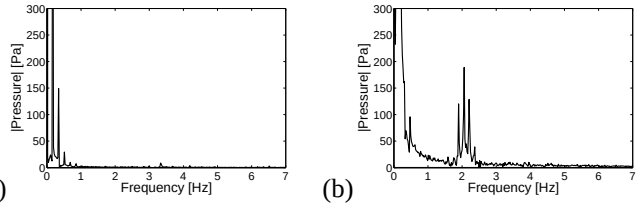

Figure 8. Frequency spectra for the pressure in point A (figure 2) for angles of incidence (a) $\alpha = 30^\circ$ and (b) $\alpha = 60^\circ$.

3.3 Pressure loads on the cylinders

Pressure distributions on the walls of the cylinders may clarify the excitation of ovalling oscillations in the silo group. Time averaged pressures provide an indication of the static deflection of the silos while fluctuating pressures represent the dynamic excitation of the silos. The fluctuating pressure coefficients along the circumference of each cylinder are determined in every time step as follows:

$$C_{\mathrm{p}}^{'}(\theta,t) = C_{\mathrm{p}}(\theta,t) - \overline{C}_{\mathrm{p}}(\theta) \tag{3}$$

To investigate the contribution of static and fluctuating pressures on the eigenmodes of the silos, the pressure coefficients can be harmonically decomposed into a series of cosine functions with circumferential wavenumber n, corresponding to the ovalling

mode shapes of the axisymmetric structure (figure 1):

$$\overline{C}_{\mathrm{p}}(\theta) = \sum_{n=0}^{\infty} \overline{C}_{\mathrm{p}}^{n} \cos(\mathrm{n}\theta + \overline{\phi}_{\mathrm{n}}) \tag{4}$$

$$C_{\mathrm{p}}^{'}(\theta,t) = \sum_{n=0}^{\infty} C_{\mathrm{p}}^{'n}(t) \cos(\mathrm{n}\theta + \overline{\phi}_{\mathrm{n}}) \tag{5}$$

For a single cylinder, this yields for every n a single value for the time averaged and a value in every time step for the fluctuating pressure.

The group configuration drastically changes the pressure distributions around the cylinders in group arrangement when compared to the single cylinder case (figure 9). On the transverse upstream corners of the group (e.g. cylinders 1 and 33 for $\alpha = 0^{\circ}$, figure 9a, or cylinders 8 and 33 for $\alpha = 60^{\circ}$, figure 9b), the highest time averaged suction pressures occur prior to the separation of the shear layer. At the lee side of the group (e.g. cylinders 24, 32 and 36 to 40 for $\alpha = 60^{\circ}$, figure 9b), pressure distributions are nearly uniform and can be related to the constant negative base pressure at the lee side of a single cylinder in cross flow. Distinct minima in the pressure distributions are observed in the narrow gaps between cylinders where the interstitial flow velocities are largest (e.g. cylinder 22 in figure 9b). At incidence angle $\alpha = 0^{\circ}$ (figure 9a), where the interstitial flow is deflected upward and downward in the upstream part of the group, the flow velocities in the gaps in the middle of the group are much lower and these minima cannot be observed.

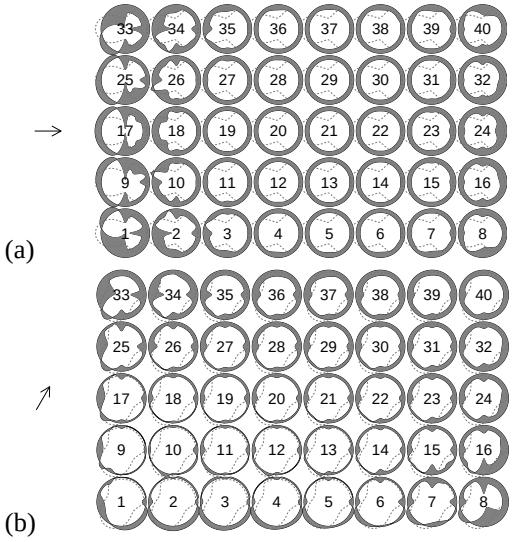

Figure 9. Time averaged pressure coefficients $\overline{C}_{\mathrm{p}}(\theta)$ for all cylinders in the group arrangement for an angle of incidence (a) $\alpha = 0^{\circ}$ and (b) $\alpha = 60^{\circ}$. Dashed lines indicate the time averaged pressure coefficient $\overline{C}_{\mathrm{p}}(\theta)$ for the single cylinder case (figure 3).

By harmonic decomposition of the time averaged pressure coefficient $\overline{C}_{\mathrm{p}}(\theta)$, it becomes clear which harmonics will contribute most to the static deflection of the silo. Figure 10 shows the variation of $\overline{C}_{\mathrm{p}}^{n}$ for $0 \leq n \leq 4$ as a function of the angle of incidence α for five typical locations in the group: the four corner cylinders (1, 8, 33 and 40), a cylinder in the middle of the group (21) and the single circular cylinder for reference. It is observed that the cylinders on the corners of the group, where the shear layer is separated, are more strongly loaded than the single cylinder: for cylinder 8 (figure 10d) contributions for higher angles of incidence ($\alpha > 60^{\circ}$) are larger while for cylinder 33 (figure 10a) this is the case for low angles of incidence ($\alpha < 30^{\circ}$). Cylinder 1 on the other hand (figure 10c) is most heavily loaded for $\alpha = 0^{\circ}$ and $\alpha = 90^{\circ}$. Remarkably, for the cylinders where the shear layer is separated, the contribution of the third and fourth harmonics ($n = 3$,$n = 4$) are much larger than for other cylinders in the group or the single cylinder case. For cylinder 40 (figure 10b), the most important contribution originates from the uniform component $\overline{C}_{\mathrm{p}}^{0}$ which can again be related to the constant base pressure at the lee side of a single cylinder, while contributions of other harmonics are much smaller than the reference values for the single cylinder. For cylinder 21 in the center of the group (figure 10e), it should be noted that apart from the uniform component, the fourth harmonic has the highest contribution for all angles of incidence, caused by the 4 distinct minima in the time averaged pressure distributions (figure 9).

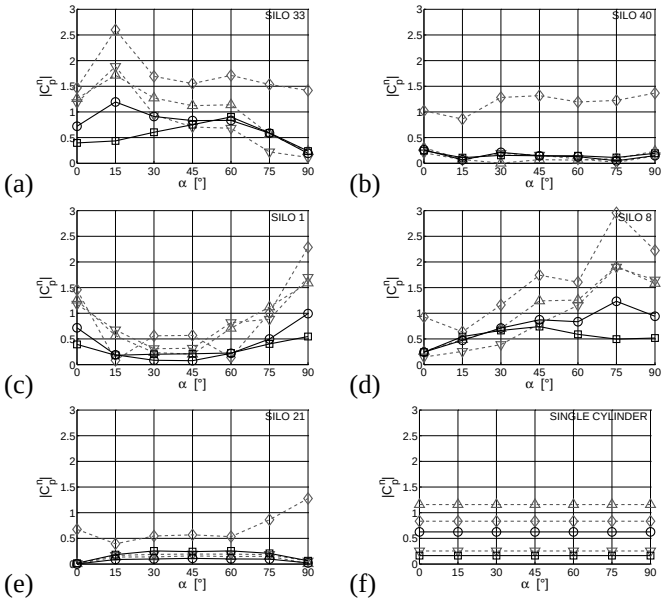

Figure 10. Amplitude $\overline{C}_{\mathrm{p}}^{0}$ ($\diamond$), $\overline{C}_{\mathrm{p}}^{1}$ ($\triangle$), $\overline{C}_{\mathrm{p}}^{2}$ ($\triangledown$), $\overline{C}_{\mathrm{p}}^{3}$ ($\bigcirc$) and $\overline{C}_{\mathrm{p}}^{4}$ ($\square$) for (a) cylinder 33, (b) cylinder 40, (c) cylinder 1, (d) cylinder 8, (e) cylinder 21, and (f) the reference single cylinder case, as a function of the angle of incidence α.

Since static, time averaged pressures are unable to trigger oscillations, the time history of the amplitudes $C_{\mathrm{p}}^{'n}(t)$ are transformed to the frequency domain by means of a FFT algorithm. Results for angle of incidence $\alpha = 30^{\circ}$ and for circumferential wave numbers $n = 3$ and $n = 4$ are shown in figure 11 for cylinders 1, 8, 21, 33 and 40. The frequency spectra for cylinders 1 and 33 (figures 11c and 11a) show no periodicities other than the low frequency contributions related to the large vortex shedding in the wake of the group. However, moving towards the lee side of the group, irregularities appear: higher frequencies also prevail in the frequency spectra for cylinders 8 and 40 (figures 11d and 11b).

This frequency content at around 3 Hz to 4 Hz indicates that the third and fourth circumferential eigenmodes of the silos (both at eigenfrequencies of 3.93 Hz) will probably be excited. Moving downstream within the group, contributions at even higher frequencies are also encountered (e.g. cylinder 21, figure 11e). For other angles of incidence, the presence of peaks in the frequency range between 3 Hz and 4 Hz confirms that the eigenmodes with the lowest eigenfrequencies, i.e. modes (1,3) and (1,4) (figure 1), will probably be excited at the lee side of the silo group.

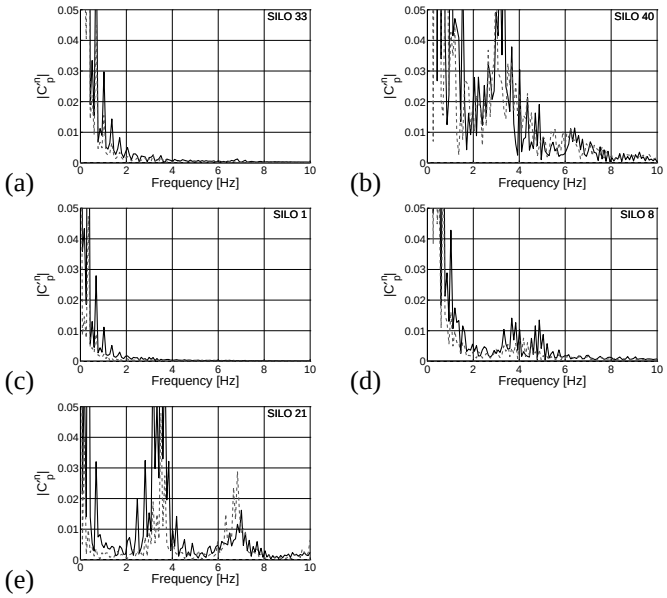

Figure 11. Frequency spectra for the amplitude of $C_p'^3$ (solid line) and $C_p'^4$ (dashed line) for (a) cylinder 33, (b) cylinder 40, (c) cylinder 1, (d) cylinder 8 and (e) cylinder 21.

Similarly, time averaged and fluctuating drag and lift forces on the cylinders in the group can be determined. For all angles of incidence, time averaged drag and lift are considerably larger at the corner silos in comparison with cylinders in the middle of the group. The reasonably high lift coefficients on the transverse corner silos where the shear layer is separated, indicate that these cylinders are pulled away from the group. Fluctuations tend to be larger at the windward side of the group.

4 OVALLING OSCILLATIONS IN THE 8 BY 5 SILO GROUP

Based on the results of the numerical simulations, the location and cause of ovalling vibrations in the silo group can be explained.

The silos near the transverse corners of the group, where the shear layer is separated, are subject to the largest time averaged pressures. Remarkably, the third and fourth circumferential harmonics in the static pressure are specifically pronounced on these corners. The combined effect of the latter with the large time averaged and fluctuating drag and lift forces near these corners, may result in observable rigid body motions of the statically deformed silos. This effect being fundamentally different from ovalling vibrations, dynamic pressure fluctuations have been studied. Harmonic decomposition and transformation to the frequency domain of the dynamic pressures show that the third and fourth ovalling eigenmodes of the silos will most likely be excited on silos at the lee side corners of the group. For certain angles of incidence, these ovalling oscillations may not only be present at the lee side corner of the inclined group but also on transverse corners of the group: e.g. silo 8 for angle of incidence $\alpha = 30^\circ$ (figure 11d). This corresponds with the observed ovalling eigenmodes with three and four circumferential wavelengths during the 2002 storm in Antwerp.

Although the underlying mechanism inducing ovalling vibrations is not fully understood at present, it is generally accepted that there are three distinct mechanisms leading to vibrations in tube arrays [8] [21]. Firstly, forces can arise due to coincidence of a structural natural frequency with the vortex shedding frequency in the tube wake. The possibility of vortex shedding in closely spaced tube arrays has been the subject of controversy for several decades [21] but is now reasonably well understood. Secondly, fluid-elastic instability is based on self-excited forces which are caused by the interaction between tube motion and fluid flow. Vibrations in a regular tube array cause the arrangement to become irregular, particularly in closely spaced arrays [18]. The fluid-elastic forces are proportional to tube displacement at the onset of instability and are superimposed by a second type of forces, proportional to tube vibration velocities. The first is typically dominant in staggered tube configurations while the second can become dominant in in-line configurations [22]. Finally, turbulent buffeting forces arise due to turbulent fluctuations of the flow pressure. These forces arise as a response to flow turbulence, either initiated upstream or induced within the array itself [8].

Considering resonance effects in the present configuration, distinction should be made between interstitial flow periodicities and classical vortex shedding around the entire group. The large difference between the natural ovalling frequencies (figure 1) and the vortex shedding frequencies in present simulations (f_{vs} in table 1), confirms that subharmonic excitation by vortex shedding is a condition neither necessary nor sufficient for the onset of ovalling [23]. Furthermore, Païdoussis et al. [24] have convincingly shown that conventional vortex shedding cannot excite ovalling oscillations of cylindrical shells in cross flow since ovalling of a single cylinder also occurs when a long splitter plate in the wake suppresses periodic vortex shedding. Although the periodicities in the interstitial flow may be very different from classical vortex shedding, these do not seem to be related to ovalling, since they occur throughout the entire group while ovalling is only observed on the corner silos. Hence, fluid-elastic instability and/or turbulent buffeting are believed to be causing the wind induced ovalling vibrations on the corners of the silo group. Although fluid-elastic instability was excluded as a cause of vibrations in an infinite rotated square tube array at $\mathrm{Re} = 1.2 \times 10^4$ by Price et al. [8], this should not be generalized for the current 8 by 5 cylinder group at a much higher Reynolds number. Turbulent buffetting, finally, may very well be triggering ovalling vibrations as well because of the large pressure fluctuations at the lee side of the group, where dynamic pressure excitation on the silos was shown to excite the lowest structural eigenmodes.

5 CONCLUSIONS

In order to elucidate the occurence of ovalling oscillations on the empty corner silos of a 8 by 5 silo group in the port of Antwerp, the post-critical flow around this closely spaced cylinder group was simulated numerically. 2D URANS simulations for the entire group were performed for 7 angles of incidence α between 0° and 90°.

The group configuration and orientation of the group drastically change the flow regime, showing similarities with the fluid flow around bluff rectangular cylinders. Differences in flow pattern and Strouhal number are due to the porosity and rounded corners of the group, the higher Reynolds number and the difference in turbulence intensity. Approximately 10% of the incident flow penetrates the group and emerges at the lee side to form local recirculation zones when the group is sufficiently inclined. These emerging interstitial flows prevent the shear layer from reattaching and eventually coalesce to form a large vortex street in the wake of the group.

The flow in the interstitial spaces of the group is somewhat similar to the flow in tube bundles (e.g. heat exchangers). Although the flow pattern is clearly different when the group is oriented parallel to the incident flow ($\alpha = 0^\circ$ or $\alpha = 90^\circ$), for an inclined orientation, the interstitial flow is very similar, following wavy paths through the array. For $\alpha = 15^\circ$ and $\alpha = 60^\circ$, at arbitrary locations in the array some irregularities in the otherwise regular wavy flow pattern are observed. This results in higher frequency periodicities in the interstitial flow which is attributed to the 2D character of the numerical simulations where spanwise velocities are suppressed.

Both static deflection (time averaged pressures) and dynamic excitation (fluctuating pressures) are considered. The silos near the transverse corners of the silo group, where the shear layer is separated, are subject to the largest static pressures for all angles of incident flow. Remarkably, the third and fourth circumferential harmonics in the static pressure are specifically pronounced for these cylinders. To explain the existence of ovalling vibrations, however, dynamic fluctuations in the pressure loading on the silos should be considered. For all angles of incidence α, dynamic pressures on the silos at the lee side of the group are seen to most likely excite the third and fourth structural eigenmodes, corresponding with the lowest eigenfrequencies. This corresponds with the visually detected ovalling eigenmodes with three and four circumferential wavelengths at the corner silos of the group during the 2002 storm in Antwerp. Based on these results, the underlying physical mechanisms producing the flow periodicities and eventually inducing the ovalling vibrations are believed to be turbulent buffeting and/or fluid-elastic instability while resonance with some periodic vortex shedding can be excluded.

ACKNOWLEDGMENTS

The research in this paper has been performed within the frame of the FWO project G.0275.08 ”Efficient analysis of fluid-structure interaction problems in structural dynamics”. The support of FWO is gratefully acknowledged.

REFERENCES

[1] BIN, *NBN EN 1991-1-4:2005 Eurocode 1: Actions on structures - Part 1-4: General actions - Wind actions*, Belgisch Instituut voor Normalisatie, April 2005.

[2] M.M. Zdravkovich, *Flow Around Circular Cylinders, Volume 1: Fundamentals*, Oxford University Press, Oxford, England, 1997.

[3] M.P. Païdoussis, S.J. Price, and H.C. Suen, “Ovalling oscillations of cantilevered and clamped-clamped cylindrical-shells in cross flow: An experimental-study,” *Journal of Sound and Vibration*, vol. 83, no. 4, pp. 533–553, 1982.

[4] D. Dooms, G. Degrande, G. De Roeck, and E. Reynders, “Finite element modelling of a silo based on experimental modal analysis,” *Engineering Structures*, vol. 28, no. 4, pp. 532–542, 2006.

[5] H.K. Versteeg and W. Malalasekara, *An Introduction to Computational Fluid Mechanics: The Finite Volume Method*, Pearson Education Limited, Essex, England, second edition, 2007.

[6] Ansys, *Theory Guide, ANSYS FLUENT Release 12.0*, Ansys Inc., April 2009.

[7] R. Mittal and S. Balachandar, “Effect of three-dimensionality on the lift and drag of nominally two-dimensional cylinders,” *Physics of Fluids*, vol. 7, no. 8, pp. 1841–1865, 1995.

[8] S.J. Price, M.P. Païdoussis, R. Macdonald, and B. Mark, “The flow-induced vibration of a single flexible cylinder in a rotated square array of rigid cylinders with a pitch-to-diameter ratio of 2.12,” *Journal of Fluids and Structures*, vol. 1, no. 3, pp. 359–378, 1987.

[9] M.M. Sitheeq, A.K.S. Iyengar, and C. Farell, “Effect of turbulence and its scales on the pressure field on the surface of a three-dimensional square prism,” *Journal of Wind Engineering and Industrial Aerodynamics*, vol. 71, pp. 461–471, 1997.

[10] S.J. Zan, “Experiments on circular cylinders in crossflow at Reynolds numbers up to 7 million,” *Journal of Wind Engineering and Industrial Aerodynamics*, vol. 96, no. 6–7, pp. 880–886, 2008.

[11] G. Schewe, “On the force-fluctuations acting on a circular-cylinder in cross-flow from subcritical up to transcritical Reynolds-numbers,” *Journal of Fluid Mechanics*, vol. 133, no. AUG, pp. 265–285, 1983.

[12] B.A. Younis and V.P. Przulj, “Computation of turbulent vortex shedding,” *Computational Mechanics*, vol. 37, no. 5, pp. 408–425, 2006.

[13] A. Travin, M. Shur, M. Strelets, and P. Spalart, “Detached-eddy simulations past a circular cylinder,” *Flow, Turbulence and Combustion*, vol. 63, no. 1–4, pp. 293–313, 2000.

[14] A. Kareem, T. Kijewski, and P.C. Lu, “Investigation of interference effects for a group of finite cylinders,” *Journal of Wind Engineering and Industrial Aerodynamics*, vol. 77–78, pp. 503–520, 1998.

[15] C.W. Knisely, “Strouhal numbers of rectangular cylinders at incidence: a review and new data,” *Journal of Fluids and Structures*, vol. 4, no. 4, pp. 371–393, 1990.

[16] J.M. Chen and C.-H. Liu, “Vortex shedding and surface pressures on a square cylinder at incidence to a uniform air stream,” *International Journal of Heat and Fluid Flow*, vol. 20, no. 6, pp. 592–597, 1999.

[17] P. Hémon and F. Santi, “On the aeroelastic behaviour of rectangular cylinders in cross-flow,” *Journal of Fluids and Structures*, vol. 16, no. 7, pp. 885–889, 2002.

[18] M.M. Zdravkovich, *Flow Around Circular Cylinders, Volume 2: Applications*, Oxford University Press, Oxford, England, 2003.

[19] J.C.R. Hunt and I. Eames, “The disappearance of laminar and turbulent wakes in complex flows,” *Journal of Fluid Mechanics*, vol. 457, pp. 111–132, 2002.

[20] C. Moulinec, M.J.B.M. Pourquié, B.J. Boersma, T. Buchal, and F.T.M. Nieuwstadt, “Direct numerical simulation on a cartesian mesh of the flow through a tube bundle,” *International Journal of Computational Fluid Dynamics*, vol. 18, no. 1, pp. 1–14, 2004.

[21] D.S. Weaver, H.Y. Lian, and X.Y. Huang, “Vortex shedding in rotated square arrays,” *Journal of Fluids and Structures*, vol. 7, no. 2, pp. 107–121, 1993.

[22] K. Schroder and H. Gelbe, “New design recommendations for fluidelastic instability in heat exchanger tube bundles,” *Journal of Fluids and Structures*, vol. 13, no. 3, pp. 361–379, 1999.

[23] A. Laneville and A. Mazouzi, “Ovalling oscillations of cantilevered cylindrical shells in cross-flow: New experimental data,” *Journal of Fluids and Structures*, vol. 9, no. 7, pp. 729–745, 1995.

[24] M.P. Païdoussis, S.J. Price, and S.-Y. Ang, “Ovalling oscillations of cylindrical shells in cross flow: A review and some new results,” *Journal of Fluids and Structures*, vol. 2, no. 1, pp. 95–112, 1988.